Geomorphology 311 (2018) 1–12

Contents lists available at ScienceDirect

Geomorphology

journal homepage: www.elsevier.com/locate/geomorph

Debris thickness patterns on debris-covered glaciers

Leif S. Anderson [a,b,c,*], Robert S. Anderson [c]

[a] Faculty of Earth Sciences, University of Iceland, 101 Reykjavík, Iceland
[b] Department of Earth Sciences, Simon Fraser University, Burnaby, B.C. V5A 1S6, Canada
[c] Department of Geological Sciences, and Institute of Arctic and Alpine Research (INSTAAR), University of Colorado, Boulder, CO 80309, USA

ARTICLE INFO

Article history:
Received 22 December 2017
Received in revised form 18 March 2018
Accepted 18 March 2018
Available online 20 March 2018

Keywords:
Headwall erosion
Debris expansion
Debris-mantled glacier
Climate change

ABSTRACT

Many debris-covered glaciers have broadly similar debris thickness patterns: surface debris thickens and tends to transition from convex- to concave-up-down glacier. We explain this pattern using theory (analytical and numerical models) paired with empirical observations. Down glacier debris thickening results from the conveyor-belt-like nature of the glacier surface in the ablation zone (debris can typically only be added but not removed) and from the inevitable decline in ice surface velocity toward the terminus. Down-glacier thickening of debris leads to the reduction of sub-debris melt and debris emergence toward the terminus. Convex-up debris thickness patterns occur near the up-glacier end of debris covers where debris emergence dominates (*ablation controlled*). Concave-up debris thickness patterns occur toward glacier termini where declining surface velocities dominate (*velocity controlled*). A convex-concave debris thickness profile inevitably results from the transition between ablation-control and velocity-control down-glacier. Debris thickness patterns deviating from this longitudinal shape are most likely caused by changes in hillslope debris supply through time. By establishing this expected debris thickness pattern, the effects of climate change on debris cover can be better identified.

1. Introduction

Surface debris thickness is a primary control of melt (e.g., Østrem, 1959). Debris thickness patterns therefore control melt patterns and glacier response to climate change (e.g., Benn et al., 2012). It follows that we must then understand what controls debris thickness patterns on glaciers. We identify two features common to debris patterns: first, mean debris thicknesses increase down-glacier, with the maximum thickness typically occurring near the terminus (Figs. 1–2; Nakawo et al., 1986; Kirkbride, 1993, 2000; Kirkbride and Warren, 1999; Shroder et al., 2000; Owen et al., 2003; Kellerer-Pirklbauer, 2008; Mihalcea et al., 2008; Wang et al., 2011; Zhang et al., 2011; Juen et al., 2014; Schauwecker et al., 2015; Anderson and Anderson, 2016). Second, debris thickness typically transitions from a decreasing rate of debris thickening down-glacier to an increasing rate of thickening down-glacier (Fig. 2A). In other words, debris thickness transitions from convex-up to concave-up down glacier; examples exist for ice-stream interaction and avalanche-type medial moraines (Fig. 2A; Glazyrin, 1975; Eyles and Rogerson, 1978; Anderson, 2000; Kirkbride, 2000; Shroder et al., 2000). What controls this commonly observed debris thickness pattern?

A variety of processes affect debris thickness patterns. Debris emergence patterns and surface velocity gradients appear to control debris patterns on all glaciers (see Nakawo et al., 1986; Kirkbride and Warren, 1999; Anderson and Anderson, 2016). The junction of two tributaries might lead to differences in debris thicknesses between the joined ice bodies owing to variable debris supply between the tributaries (e.g., Mihalcea et al., 2008; Gibson et al., 2017). Nonsteady debris delivery to glaciers, most clearly manifested as landslide deposits on glacier surfaces, leads to local increases in debris thickness (e.g., Eyles and Rogerson, 1978; Deline, 2005; Vacco et al., 2010; Reznichenko et al., 2011). Currently, debris covers around the globe are expanding because of climate warming (e.g., Kirkbride, 1993; Popovnin and Rozova, 2002; Deline, 2005, 2009; Stokes et al., 2007; Bolch et al., 2008; Kellerer-Pirklbauer, 2008; Shukla et al., 2009; Kirkbride and Deline, 2013; Janke et al., 2015; Minora et al., 2015; Gibson et al., 2017; Azzoni et al., 2018). We distill these apparent controls on debris patterns into four categories: (i) the basic physics and structure common to all debris-covered glaciers that we refer to as *intrinsic* processes (debris emerges in the ablation zone, debris advects down-glacier, and thick debris reduces melt, etc.); (ii) the glacier geometry (hypsometry, variable bed slope, etc.) (iii) the spatial variability and history of debris supply to the glacier; and (iv) the history of climate.

* Corresponding author at: Faculty of Earth Sciences, University of Iceland, 101 Reykjavík, Iceland.
E-mail address: leif@hi.is (L.S. Anderson).

https://doi.org/10.1016/j.geomorph.2018.03.014
0169-555X/

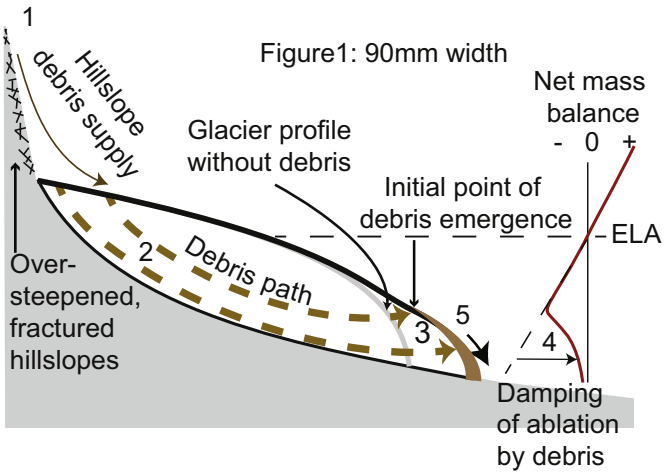

Fig. 1. Schematic of the debris-covered glacier system. The equilibrium-line-altitude (*ELA*) separates the zone of net accumulation above from the zone of net ablation below. (1) Above-glacier hillslopes deliver debris that is deposited on the glacier. (2) Debris is transported through the glacier following the trajectory of the ice in which it is embedded. (3) Debris melts out of the glacier (emerges) in the ablation zone onto the glacier surface. (4) Sub-debris ablation rates decline rapidly as debris thickens, altering the local mass balance. (5) Debris on the glacier surface is transported toward the terminus where it is deposited in the foreland.

If we isolate the effects of *intrinsic* processes and geometric controls on debris patterns, we will be more effective at identifying the records of climate and hillslope erosion change in debris patterns. For example, if the typical convex-concave thickness profile is the simple consequence of *intrinsic* processes, then deviation from that form will reveal the effects of variable climate and hillslope erosion (see Deline, 2009's Fig. 3, as an example). If we hold climate steady with debris supply uniform in space and steady in time and use the simplest glacier geometry, what is the expected debris thickness pattern on a glacier?

As a complement, we also assess the importance of debris thickness patterns in controlling other seemingly universal features of debris-covered glaciers. For example, observed surface velocity gradients tend to be lower on debris-covered glaciers than debris-free glaciers, independent of the effects of modern warming (e.g., Konrad and Humphrey, 2000; Scherler et al., 2011; Banerjee and Shankar, 2013; Anderson and Anderson, 2016). And thick, continuous debris leads to increased glacier lengths (Ogilvie, 1904; Clark et al., 1994; Konrad and Humphrey, 2000; Shroder et al., 2000; Zech et al., 2005; Vacco et al., 2010; Yde and Paasche, 2010; Scherler et al., 2011; Menounos et al., 2013).

We derive a steady state analytical model that simplifies the relationship between debris, melt, and ice dynamics and includes basic physical processes common to all debris-covered glaciers. We then provide basic, physical explanations for the convex-concave debris pattern that we use to evaluate (analytically and numerically) modeled and observed debris patterns. While extant debris-covered glaciers are clearly changing in time, steady state modeling establishes a reference state from which we can identify the effects of transience in the debris-covered glacier system (see Konrad and Humphrey, 2000; Banerjee and Shankar, 2013; Rowan et al., 2015; Anderson and Anderson, 2016, for similar steady state assumptions).

2. Analytical model description

We first describe an analytical, debris-free glacier model. We consider a linear valley

$$z = z_{max} - Sx \quad (1)$$

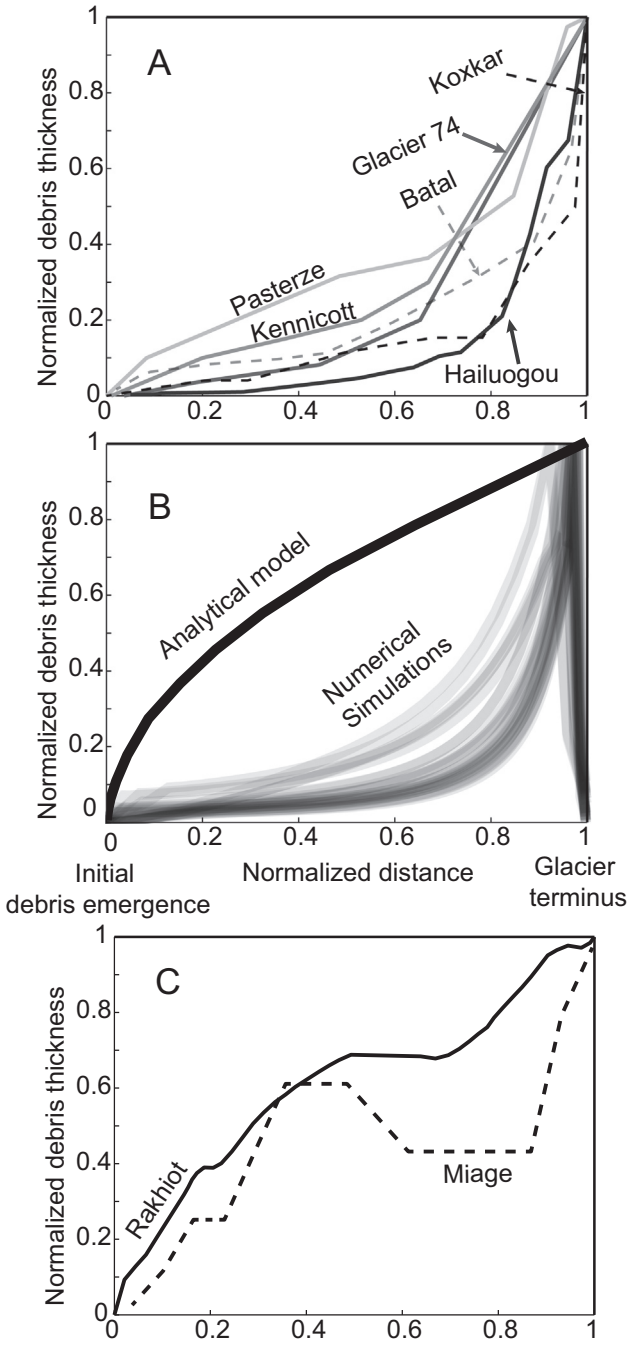

Fig. 2. Longitudinal debris thickness profiles from debris-covered glaciers and debris-covered glacier models. (A) Measured debris thickness profiles normalized by the maximum debris thickness that show a convex- concave-up debris thickness pattern (data from Kellerer-Pirklbauer, 2008; Wang et al., 2011; Zhang et al., 2011; Anderson, 2014; Patel et al., 2016; Huang et al., 2018). See Glazyrin (1975) and Zhang et al. (2016) for more examples showing the convex- concave-up debris thickness pattern. Glacier centerline distance is normalized by the length of the debris-covered portion of the glacier. (B) Steady state analytical model debris thickness profile (solid black) and debris thickness profiles from 144 numerical model simulations run to steady state (from Anderson and Anderson, 2016). (C) Measured debris thickness profiles normalized by the maximum debris thickness that deviate from the convex- concave-up debris thickness pattern (Owen et al., 2003; Mihalcea et al., 2008). Other debris thickness profiles from Owen et al. (2003) show the convex- concave-up debris thickness pattern.

where z is the elevation, z_{max} is the maximum elevation of the valley, S is the slope, and x is the down-valley distance ($x = 0$ the valley head; Fig. 3).

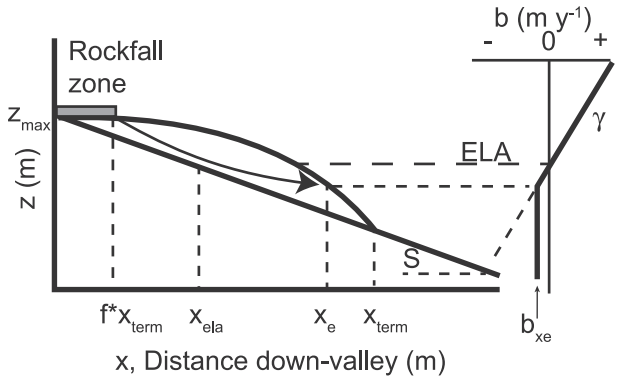

Fig. 3. Schematic of analytical model set-up. Linear glacier valley is subjected to linear clean ice mass balance profile. Glacier is shown in the absence of debris feedbacks, with predictable glacier length x_{term}. Rockfall zone length, point of emergence of debris in ablation zone, and the clean ice balance at the point of emergence are depicted.

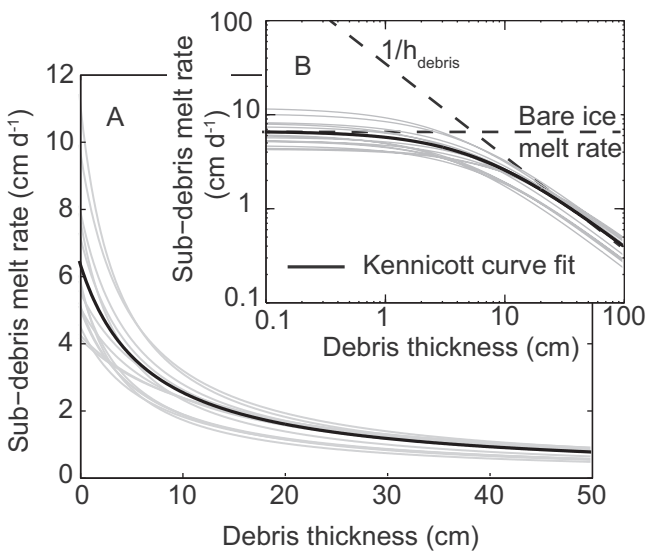

Fig. 4. Hyperbolic dependence of sub-debris melt rate on debris thickness. (A) The strong dependence of sub-debris melt rate on debris thickness, following Eq. (7) (mean h_* is 0.066 ± 0.029 m (1st dev.) and ranges from 0.03 to 0.13 m) (see Anderson and Anderson, 2016). (B) Same debris thickness profiles as in A but in log-log space to highlight the hyperbolic relationship between the melt rate and debris thickness.

2.1. Clean ice mass balance pattern

We assume a distribution of annual net mass balance within the valley that is the sum of total annual melt and snow accumulation. For many alpine glaciers, the net mass balance varies linearly with elevation. The clean ice mass balance b is therefore

$$b = \gamma(z - ELA) \tag{2}$$

where z is elevation, γ the mass balance gradient, and ELA (equilibrium line altitude) is the elevation at which the net mass balance is zero. For the debris-covered portion of the modeled glacier, the clean ice mass balance refers to the hypothetical mass balance if debris is not present to perturb melt.

2.2. Steady state pattern of debris-free ice discharge

Given the profile of mass balance $b(z)$ and the valley profile, we transform $b(z)$ into $b(x)$, the mass balance profile as a function of distance down valley to

$$b = \gamma[z - ELA] - \gamma S x \tag{3}$$

Mass balance declines linearly down-valley (following Anderson et al., 2006). Along a one-dimensional flowline in a glacier of uniform width, conservation of ice may be written as

$$\frac{\partial H}{\partial t} = b - \frac{\partial Q}{\partial x} \tag{4}$$

where H is ice thickness, b is the clean ice mass balance, and Q is ice discharge per unit contour length. In steady state ($\partial H/\partial t = 0$) the pattern of ice discharge may be calculated by integrating Eq. (4):

$$Q = \int_0^x b\,dx \tag{5}$$

The terminus is the location where discharge equals zero. The steady terminus position in the debris-free case is simply

$$x_{term} = \frac{2(z_{max} - ELA)}{S} \tag{6}$$

2.3. The effect of debris on surface ablation

Surface debris can greatly perturb melt rates (Fig. 4). We assume that heat is transferred through the debris layer by conduction, in which case sub-debris melt depends on the temperature gradient ~$(T_s$-$T_{ice})/h_{debris}$ (where T_s is the debris surface temperature, T_{ice} is the temperature at the ice-debris interface, and h_{debris} is the debris thickness; e.g., Nicholson and Benn, 2006). We expect sub-debris melt to decline inversely with debris thickness, i.e., be hyperbolic (Anderson and Anderson, 2016). We neglect the melt-amplifying effects of very thin debris for simplicity and represent the damped sub-debris mass balance b' by debris thickness h_{debris} using

$$b' = b\left(\frac{h_*}{h_* + h_{debris}}\right) \tag{7}$$

(Anderson and Anderson, 2016; Fig. 4). Here h_* is a characteristic length scale that controls how rapidly sub-debris melt asymptotes toward zero melt and is defined by

$$h_* = \frac{k\overline{T_s}}{(1-\phi)L\overline{T_a}f_{pdd}\rho_i} \tag{8}$$

where k and ϕ are thermal conductivity and porosity of the debris cover, ρ_i and L the density and latent heat of fusion of ice respectively, $\overline{T_s}$ the average debris surface temperature, $\overline{T_a}$ the average screen-level air temperature, and f_{pdd} is a positive degree day factor relating air temperature and the clean ice melt rate (e.g., Mihalcea et al., 2006). In this formulation, sub-debris melt rates approach bare-ice melt rates b as debris thins (here $h_{debris} \ll h_*$) and asymptote toward zero melt rate as debris thickens ($h_{debris} \gg h_*$). We use h_* values based on empirical fits from Anderson and Anderson (2016); ($h_* = 0.066$ m in all simulations), though the specific choice does not affect our conclusions. We neglect the local two-dimensional effects of surface streams, surface lakes, thermokarst, and ice cliffs that lead to complex local topography and melt rate fields. We reproduce the observed debris patterns without invoking these effects, suggesting that they play a secondary, local role in controlling debris thickness patterns, though they are important for the current wasting of debris-covered glaciers (e.g., Buri et al., 2016).

2.4. Analytical debris-covered glacier model

We derive the analytical debris-covered glacier model by reducing the clean ice mass balance $b(x)$ as a function of surface debris thickness

(Fig. 5). The debris-altered mass balance then adjusts the discharge pattern inferred ice thickness, and surface velocity patterns (Fig. 6). We make the following simplifying assumptions required for derivation: (i) we assume that the clean ice mass balance is uniform down-glacier from the point of debris emergence (Fig. 3). When debris is thick, this choice has a negligible effect (Fig. 5A). Analytical sub-debris melt patterns have similar shapes to modeled sub-debris melt profiles that allow variable clean ice melt rates (Figs. 5A and 7B). (ii) We assume that the concentration of debris in the debris-covered portion of the glacier is uniform. In real glaciers, englacial debris concentrations are not uniform because of variable velocities, snow accumulation rates, and debris deposition patterns (see Anderson and Anderson, 2016). This assumption does not affect the conclusions drawn from the model as similar debris thickness convexities would result with a more complicated representation of englacial debris. (iii) We assume that debris thickness is independent of velocity gradients by calculating debris thicknesses using a uniform surface velocity. While this assumption is not valid for real debris-covered glaciers, its inclusion allows us to later differentiate between the effects of debris emergence and surface velocity gradients on debris thickness profiles.

Conclusions drawn from the analytical model are parameter independent (as long as the sign is correct and mean debris thickness is larger than a few centimeters) as can be seen from the governing equations described below. While the choice is arbitrary, we choose parameters based on the Khumbu region of the Himalaya (Table 1 and citations within). Where congruent parameters exist between the analytical and numerical model, we use values previously chosen by Anderson and Anderson (2016). The conclusions drawn from the numerical model are also parameter independent.

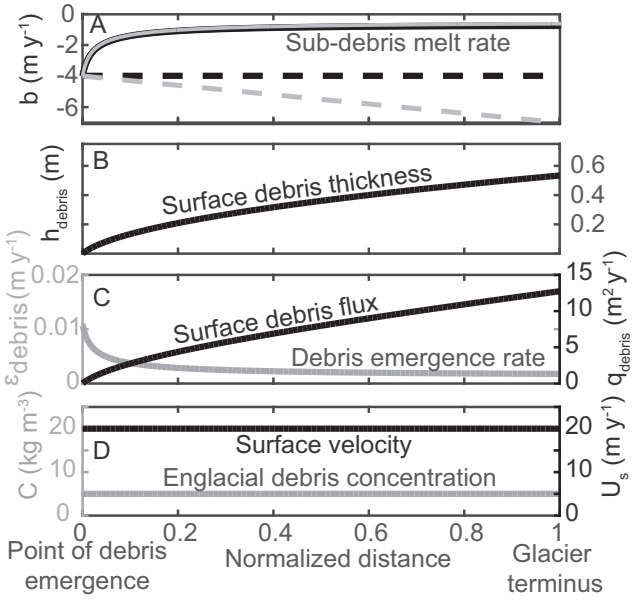

Fig. 5. Ice melt and debris thickness patterns for our analytical model and conditions leading to convex-up debris thickness profiles. Melt rate, debris thickness, debris emergence, debris flux, glacier suface velocity, and englacial debris concentration are constant in time (steady state). Distance is normalized by the length of the debris-covered portion of the glacier. (A) Clean ice mass balance (dashed) and sub-debris melt rate profiles for vaiable englacial debris concentrations. The case with variable clean ice mass balance in the debris-covered portion (grey). The case with uniform clean ice mass balance in the debris-covered portion (black). (B) Longitudinal debris thickness pattern showing the typical down-glacier thickening of surface debris. Same debris thickness profile as black line in Fig. 2B. (C) Glacier surface debris flux q_{debris} and debris emergence rate ε_{debris}. Even with uniform C and U_s fields, the the emergence rate declines toward the terminus. (D) Uniform englacial debris concentration and U_s fields. We employ the hyperbolic dependence of melt rate on debris thickness (Eq. (7); Fig. 4).

Debris is typically deposited on glaciers in the accumulation zone and transported through the glacier where it melts out in the ablation zone (Fig. 1). Surface debris then perturbs the local melt rate as the debris is transported down-glacier and off glacier at the terminus. Debris deposited on the glacier surface in the accumulation zone is incorporated into the glacier (Fig. 1). Near-surface englacial debris concentration (in units of kg m^{-3}) in the accumulation zone is governed by $C_0 = d_{flux}/b$, where d_{flux} (in units of kg m^{-2} y^{-1}) is the mass flux (supply) of debris delivered to the glacier surface. Debris supply is controlled by the height, the backwearing rate of the hillslope, and the above-glacier catchment geometry (Fig. 1; Scherler et al., 2011; Anderson and Anderson, 2016). In our model, we dictate the debris input pattern by defining a rockfall length (similar to debris deposition zone length in Anderson and Anderson, 2016), which is the distance from the headwall to the down-glacier limit of rockfall (Fig. 1).

Ice velocity fields control the trajectories of debris-laden ice. Based on our assumptions, ice trajectories underlying debris-free regions are symmetric about the *ELA* (Fig. 1). This requires that the distance from the end of the rockfall zone to the *ELA* equals the distance from the *ELA* to the initial point of debris emergence in the ablation zone (Fig. 1). The initial point of debris emergence is the first location down-glacier from the *ELA* where debris emerges onto the glacier surface. Specification of the rockfall pattern in the ablation zone therefore constrains the pattern of debris emergence in the ablation zone. We assume uniform near-surface englacial debris concentrations C from the point of initial debris emergence down-valley (Fig. 1). The specific value of C chosen does not affect our conclusions.

2.5. Steady state debris cover patterns

In the ablation zone, the rate of change of surface debris thickness in one-dimension may be written

$$\frac{\partial h_{debris}}{\partial t} = \frac{Cb'}{(1-\phi)\rho_r} - \frac{\partial (U_s h_{debris})}{\partial x} \tag{9}$$

where b' is the sub-debris ice melt rate, U_s is the down-glacier surface speed, and ρ_r is the density of rocks comprising the debris cover (e.g., Nakawo et al., 1986; Naito et al., 2000). The first term on the right-hand side is a local debris emergence rate ε_{debris} (in units of m y^{-1}), and the second represents the thickening or thinning rate of debris caused by down-valley gradients in the surface debris discharge $U_s h_{debris}$. For the analytical model, we assume a uniform U_s field in the debris-covered portion of the glacier so the right-hand term in Eq. (9) is neglected.

In steady state, $\partial h_{debris}/\partial t = 0$ and the governing equation for surface debris thickness evolution in time (Eq. (9)) reduces to

$$\frac{Cb'}{(1-\phi)\rho_r} = \frac{\partial (U_s h_{debris})}{\partial x} \tag{10}$$

In steady state, the rate at which debris emerges onto the glacier surface must match the down-valley gradient of surface debris discharge. The surface debris thickness h_{debris} is dependent on the coevolution of variables (C, b', and U_s) that are themselves dependent on debris thickness h_{debris}.

2.5.1. Steady state surface debris pattern: neglecting surface velocity gradients

To derive the analytical model, we assert uniform surface velocities and englacial debris concentrations (Fig. 5). This produces convex-up debris thickness patterns. We also assume that the clean ice mass balance (hypothetical mass balance if no debris was present) on the debris-covered ice is uniform and equal to the balance at the point of emergence of debris x_e. The location of the point of emergence is governed by the down-glacier margin of the debris input field in the

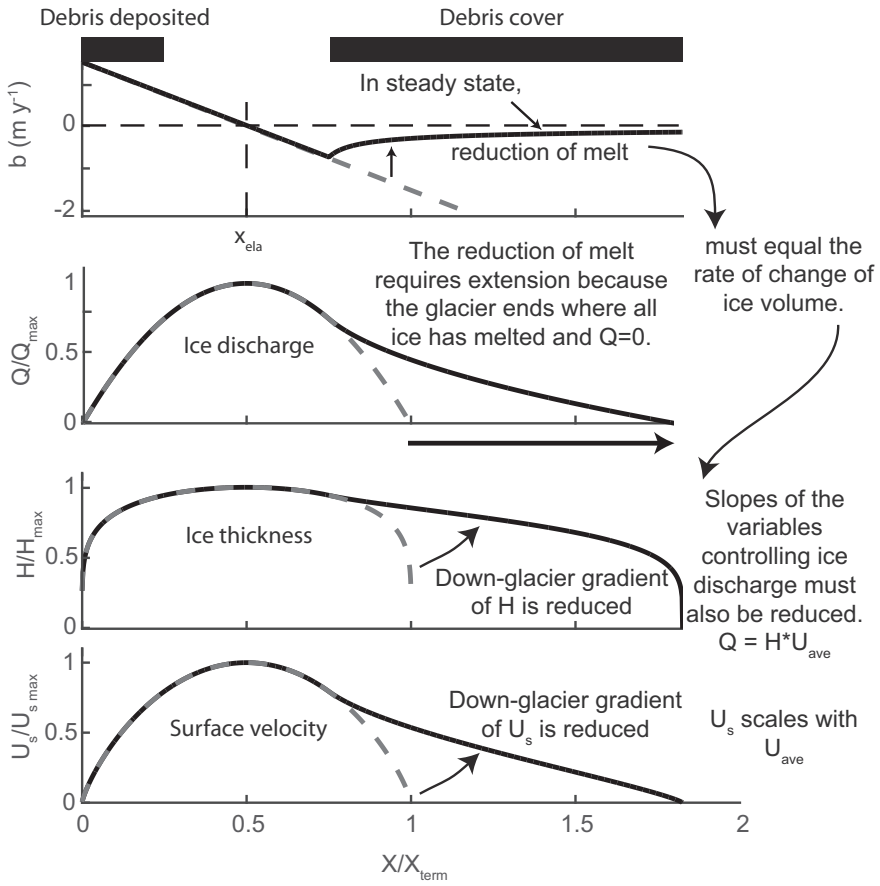

Fig. 6. Explanation of the effect of debris on glacier geometry from analytical model results. From the top to the bottom profiles of surface mass balance, ice discharge, ice thickness, and glacier surface velocity for debris-free (dashed) and debris-covered cases. Horizontal distances are normalized by the debris-free terminus position x_{term}. U_{ave} is the average velocity with depth in the glacier.

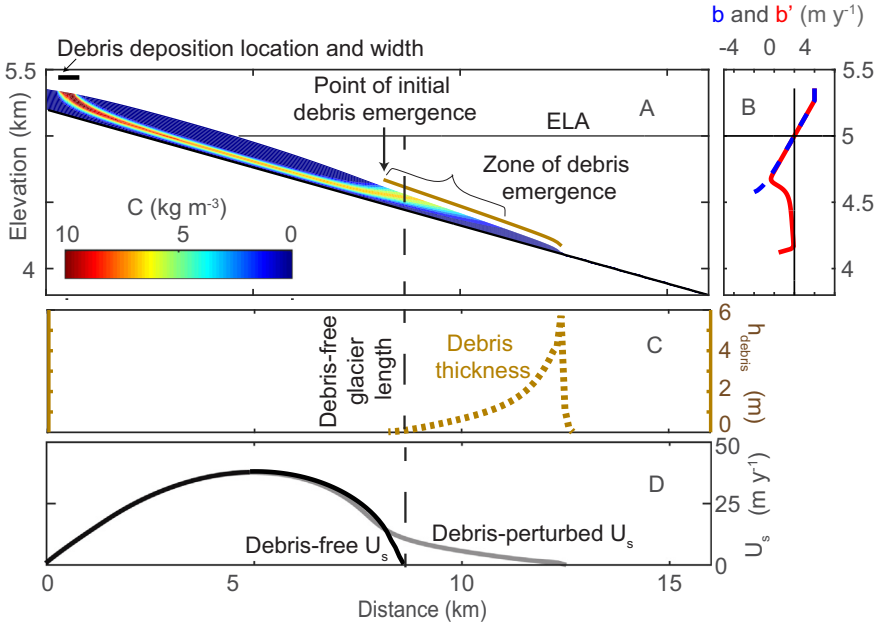

Fig. 7. Results from a numerical debris-covered glacier model (after Anderson and Anderson, 2016). (A) Englacial debris concentration that is nonuniform in the glacier interior in the debris-emergence zone; this contrasts with assumptions made in the analytical model. (B) Mass balance profiles. The blue line is the debris-free mass balance profile, and the red line is the debris-perturbed mass balance profile. (C) Surface debris thickness. (D) Surface velocity. Black: the debris-free glacier; grey: the debris-perturbed glacier. Both modeled glaciers are in steady state with the same climate (see panel B).

Table 1
Parameter definitions and values (* signifies parameters that match those applied to the numerical model of Anderson and Anderson, 2016; other parameters referenced to Anderson and Anderson, 2016 without an * are based off of that study but are not exactly those applied to the numerical model).

Parameters	Name	Reference	Min	Base	Max	Units
ELA	Equilibrium-line Altitude*	Wagnon et al. (2013)		5000		m
γ	Surface mass balance gradient*	Wagnon et al. (2013)		0.0075		y^{-1}
z_{max}	Maximum bed elevation*	Scherler (2014)		5200		m
S	Bed slope*	Scherler (2014)		8.%		
C	Englacial debris concentration	Anderson and Anderson (2016)		5.		kg m^{-3}
ρ	Rock density*	Anderson and Anderson (2016)		2650		kg m^{-3}
ϕ	Porosity*	Anderson and Anderson (2016)		0.3		
h_*	Characteristic debris thickness*	Anderson and Anderson (2016)		0.065		m
f	Rockfall fraction	Anderson and Anderson (2016)		0.25		
U_s	Glacier surface speed	Anderson and Anderson (2016)	0	20	50	m y^{-1}

accumulation area x_d. Defining that location as $x_d = fx_{ela}$, where f is the fractional distance to the x-position of the ELA (Fig. 3), the point of emergence is symmetrical about the x_{ela} and may be written as

$$x_e = x_{ela}(2-f) \tag{11}$$

We take $b(x > x_e) = b(x_e) = b_{xe}$. In steady state with the assumptions described above, Eq. (9), representing conservation of debris, becomes

$$\frac{dh_{debris}}{dx} = \frac{\alpha}{h_* + h_{debris}} \tag{12}$$

where

$$\alpha = \frac{Cb_{x_e}h_*}{(1-\phi)\rho_r U_s} \tag{13}$$

is a constant with units of length. The solution to this equation is

$$h_{debris} = h_*\left[\sqrt{1+\frac{2b_{xe}Cx'}{(1-\phi)\rho_r h_* U_s}}-1\right] = h_*\left(\sqrt{1+(x'/x_*)}-1\right) \tag{14}$$

where $x' = x\text{-}x_e$ is the distance beyond the debris emergence site, and x_* is a characteristic length scale for thickening of debris:

$$x_* = h_*\left(\frac{(1-\phi)\rho_r U_s}{2Cb_{x_e}}\right) \tag{15}$$

2.6. Steady state sub-debris melt rate

With the surface debris pattern derived above, we can extract an equation for sub-debris mass balance as a function of distance within the debris-covered portion of the glacier. The perturbed mass balance is

$$b' = b\frac{h_*}{h_* + h_{debris}} = b_{x_e}\frac{h_*}{h_* + h_*\left(\sqrt{1+\frac{x'}{x_*}}-1\right)} \tag{16}$$

This may be simplified to

$$b' = b_{x_e}\frac{1}{\sqrt{1+\frac{x'}{x_*}}} \tag{17}$$

This equation is illustrated in Fig. 5A. Sub-debris ablation declines with distance down-valley. For most parameter choices, the insulating effect of debris dominates ice ablation down-valley (Fig. 5A).

To set the scale x_* for the mass balance pattern, we require an expression for the mass balance at the point of emergence, which is the clean ice mass balance assumed at all lower elevations. Given the linear dependence of the mass balance with elevation, the mass balance at the emergence point is

$$\begin{aligned} b_{x_e} &= \gamma(z_{max}-ELA)-\gamma S[x_{ela}(2-f)] \\ &= \gamma(z_{max}-ELA)-\gamma S\left[\frac{(z_{max}-ELA)}{S}(2-f)\right] \end{aligned} \tag{18}$$

which simplifies to

$$b_{x_e} = \gamma(1-f)(z_{max}-ELA) \tag{19}$$

2.7. Steady state solution for ice discharge of debris-covered ice

In steady state the ice discharge must equal the integral of the mass balance with respect to horizontal distance, which for the region of debris cover becomes

$$Q(x>x_e) = Q_{x_e} - \int_{x_e}^{x} b'dx. \tag{20}$$

We expect the ice discharge to decline monotonically in the ablation zone, as in the debris-free case (Fig. 6). We first evaluate the ice discharge at the point of debris emergence Q_{xe}. Integrating the mass balance profile to the position x_e yields

$$Q_{x_e} = \gamma\left[(z_{max}-ELA)x_e - \frac{S}{2}x_e^2\right] \tag{21}$$

in which we use the bare ice mass balance profile. Next, we must evaluate the integral of our expression for the debris-perturbed mass balance in Eq. (17) (to solve the second term on the right side of Eq. (20)). Eq. (20) becomes

$$Q_{x'} = Q_{x_e} - b_{x_e}\int_0^{x'}\frac{1}{\sqrt{1+\frac{x'}{x_*}}}dx = b_{x_e}x_*^{\frac{1}{2}}\int_0^{x'}\frac{1}{(x_*+x')^{1/2}}dx \tag{22}$$

Evaluation of the integral and application of its limits result in

$$Q_{x'} = Q_{x_e} - 2b_{x_e}x_*^{1/2}\left[(x_*+x')^{1/2} - x_*^{1/2}\right] \tag{23}$$

The pattern of ice discharge down glacier from the point of debris emergence becomes

$$Q_{x'} = \gamma\left[(z_{max}-ELA)x_e - \frac{S}{2}x_e^2\right] - 2b_{x_e}x_*^{1/2}\left[(x_*+x')^{1/2} - x_*^{1/2}\right] \tag{24}$$

From this ice discharge pattern (Fig. 6), we now calculate ice thickness and surface speed. Because Q scales with surface slope to the 3rd power and with H to the 5th (when asserting Glen's flow law with

$n = 3$), we assume that variations in ice thickness dominate over variations in surface slope. We therefore assume a constant surface slope in our estimates of H and U_s (e.g., Konrad and Humphrey, 2000). We also assume zero contribution from basal sliding to ice discharge. It follows that ice thickness can be approximated as 1/5th power of ice discharge. On the other hand, since ice discharge ~H^5, and $U_s \sim H^4$, glacier surface speed can be approximated as the 4/5 power of the ice discharge. Analytical estimations of H and U_s show a similar shape to those derived numerically from Anderson and Anderson (2016). We compare steady state analytical glaciers with and without debris cover (Fig. 6). Down-glacier from the point of initial debris emergence, ice discharge, ice thickness, and surface velocity all display reduced gradients (Fig. 6).

3. Steady state numerical debris thickness patterns

We also evaluate the shape of previously published numerical debris thickness profiles from Anderson and Anderson (2016) (Figs. 2B and 7). Unlike the analytical model (closed form solution), the numerical model (requires time-stepping) links ice dynamics, debris transport, and debris modulation of melt as they change in time. In particular, the numerical model allows for the coevolution of internal deformation (via Glen's flow law) and sliding with englacial and surface debris advection, all coupled to sub-debris melt. The numerical model incorporates a variable clean ice mass balance profile through the debris-covered portion of the glacier and is run on a linear bed slope. Contrary to the analytical model, the numerical model allows for the nonuniform distribution of debris within the glacier (Fig. 7).

The convex-concave debris pattern arises in all 144 numerical simulations from Anderson and Anderson (2016). A wide range of debris input locations (glacier head to toe) and headwall erosions rates (1 to 8 mm y^{-1}) are explored. Additional parameters varied include: the width of debris deposition zone (100 to 1600 m), the rate at which debris leaves the glacier (by factors of 0 to 10 from the toe clean ice melt rate), the characteristic debris thickness (0.025 to 0.165 m), the debris porosity (0.18 to 0.43), and the bed slope (4% to 20%). Anderson and Anderson (2016) also showed that debris-covered glaciers are highly sensitive to changes in headwall erosion rate.

4. Intrinsic controls of debris thickness patterns

We now step back from the analytical and numerical models and engage in a thought experiment to understand the origins of down-glacier debris thickening and convex-concave debris thickness patterns.

4.1. Thickening of debris down-glacier

Integrating both sides of Eq. (10) and rearranging leads to a relationship for the steady state h_{debris} as a function of distance down-valley from the point of emergence:

$$h_{debris}(x) = \frac{1}{U_s}\int_{x_e}^{x} \frac{Cb'}{(1-\phi)\rho_r}\,dx \tag{25}$$

As surface velocity declines, debris thickness increases; and because debris typically cannot leave the glacier surface, debris thickness also increases down-glacier.

4.2. Convex-up debris patterns: ablation controlled

We start with the thought experiment where U_s and C are uniform down-glacier from the point of initial debris emergence (as in the analytical model). The surface debris thickness pattern reflects the integral of the debris emergence rate down-glacier (Eq. (25); Fig. 5). The rate of debris thickening declines down-glacier because the emergence rate declines as debris thickens: a convex-up profile results. This implies that a convex-up debris thickness profile should occur where surface velocity gradients are low and the melt out of debris dominates (Fig. 9). We refer to this case as *ablation controlled*.

4.3. Concave up debris patterns: velocity controlled

Debris emergence is negligible if there is no debris within the glacier or if sub-debris melt rates are small. In such cases Eq. (9) reduces to

$$\frac{\partial h_{debris}}{\partial t} = \frac{\partial (h_{debris} U_s)}{\partial x} \tag{26}$$

Solving for h_{debris} by taking the integral of Eq. (10) with respect to x leads to

$$h_{debris}(x) = \frac{q_e}{U_s} \tag{27}$$

where q_e is the surface parallel flux of debris at the down-glacier end of the emergence zone (where the emergence rate declines to zero; see Glazyrin, 1975). Here q_e is constant with respect to x and is the integral of emergence rate. Hence

$$q_e = \int_{x_e}^{x_{e_{end}}} \frac{Cb'}{(1-\phi)\rho_r}\,dx \tag{28}$$

with units of (m^2 y^{-1}), where $x_{e_{end}}$ is the location of the end of the debris emergence zone. The inverse of the surface speed $1/U_s$, controls the surface debris thickness pattern but is modified by the constant q_e (Fig. 8; where we apply hypothetical U_s patterns to Eq. (27)). Because surface velocities tend to monotonically decline in the ablation zone, debris thickness will take on a concave-up pattern in regions where the emergence rate is small (Fig. 9; *velocity control*). Debris will thicken more rapidly down-glacier the more rapidly the surface velocity declines (Fig. 8).

In steady state, the only other viable explanation for concave-up patterns of debris thickness is nonuniform englacial debris concentrations C that increase toward the glacier terminus (e.g., Kirkbride and Deline, 2013). We applied various patterns of englacial debris concentration that increase down-valley to Eq. (27) but were unable to produce concave-up debris patterns without declining surface velocities.

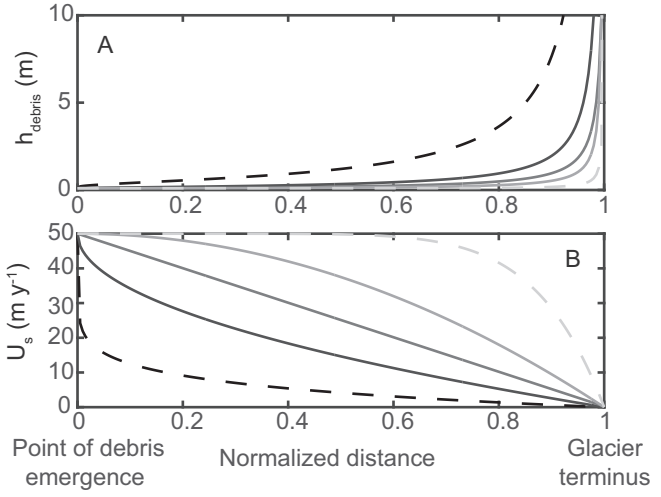

Fig. 8. Typical down-glacier debris thickness patterns when velocity dominates. (A) Sensitivity of down-glacier debris thickness pattern to assumed surface velocity patterns. The pattern of surface debris thickness is concave-up as long as the surface velocity decreases toward the glacier toe. (B) Surface speeds leading to the surface debris patterns in (A), with matching line styles.

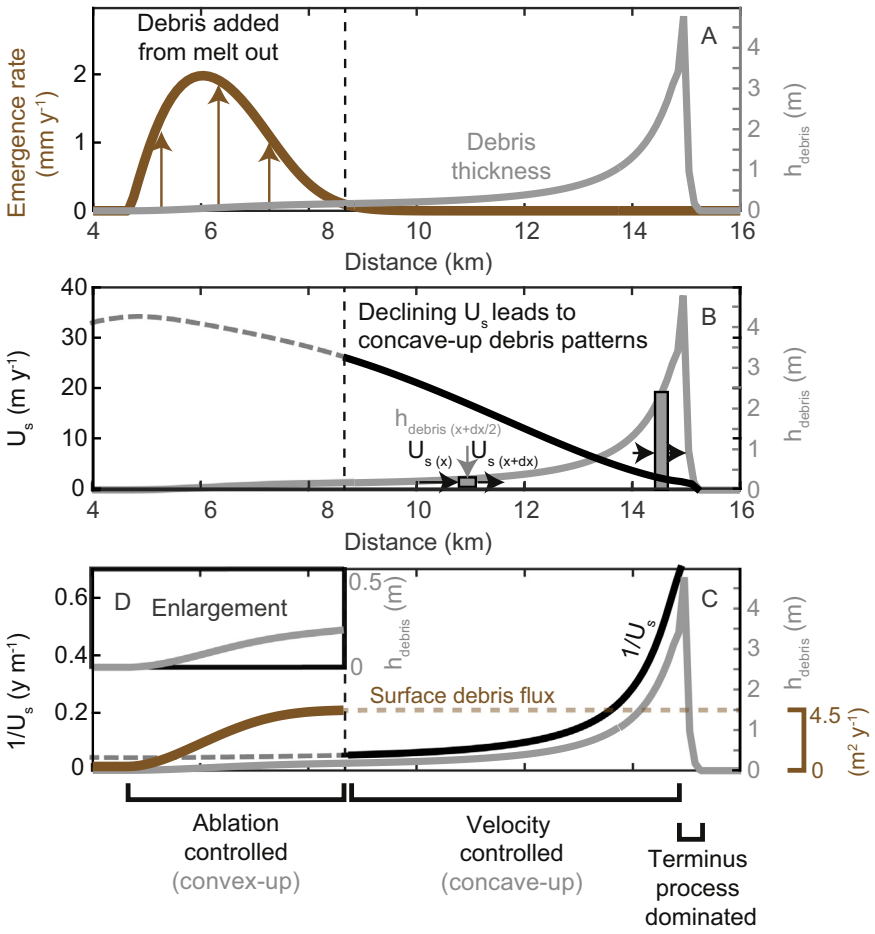

Fig. 9. Controls on steady state debris thickness patterns using numerical model output from Anderson and Anderson (2016). (A) Debris emergence rate and debris thickness. (B) Surface velocity and debris thickness. (C) Comparison of the down-glacier surface debris flux and $1/U_s$. (D) Blown up portion of the debris thickness profile in (A–C). Note the similar shapes of the surface debris flux and the surface debris thickness patterns where debris is emerging.

5. Discussion

We primarily consider the *intrinsic* controls on debris thickness patterns in the first four sections of the discussion. In the last section, we discuss the effects of glacier geometry, climate change, and variable hillslope debris supply on debris patterns in comparison with the *intrinsic* effects.

5.1. Why do modeled and observed debris thicknesses increase toward glacier termini?

The analytical, numerical, and observed debris thickness patterns all increase down-glacier (Figs. 2, 5, 7–9). For the analytical and numerical models, this increase is independent of the pattern and rate of steady debris input or differences in parameters. The analytical model shows that debris thickness increases down-glacier because the glacier surface acts as a conveyor belt: debris can only be added as it is advected toward the terminus. Debris also thickens down-glacier because surface velocities tend to monotonically decline toward zero, more debris is transported into a fixed cell than is transported out, leading to a down-glacier thickening of debris (Figs. 2, 7–9). These two processes lead to the thickening of debris down-glacier (e.g., Nakawo et al., 1986; Kirkbride and Warren, 1999; Kirkbride, 2000).

While surface debris can fall into crevasses and moulins, these processes are secondary to the two mentioned above considering that all debris patterns we know of increase down-glacier (Fig. 2). Some down-glacier debris thickening may be counteracted by debris compaction. Compaction must be a secondary effect as debris thicknesses still increase by magnitudes that greatly outweigh the possible effects of compaction: at an extreme, compaction could lead to a 40% reduction in debris thickness down-glacier (e.g., Anderson and Anderson, 2016).

In steady state, we expect portions of glaciers with higher surface velocities to have thinner debris cover than portions of glaciers with lower surface velocities (Eq. (25)). This implies that smaller glaciers with low surface velocities will support thicker debris covers closer to the point of initial debris emergence than larger glaciers with higher velocities near the point of debris emergence, an inference supported by Kirkbride and Deline (2013).

5.2. Why do debris patterns have a characteristic convex-concave form?

Debris pattern curvature reflects the relative importance of debris emergence rates and surface velocity decline down-glacier (Fig. 9). The analytical model can only produce convex-up debris patterns because it includes debris emergence but neglects surface velocity gradients (Fig. 5). Convex-up debris patterns occur where surface velocities are large, velocity gradients are small, and emergence rates are high. They should therefore be expected closer to the *ELA* where maximum ablation rates typically occur on debris-covered glaciers (*ablation controlled*; Figs. 6–7, 9).

Convex-up debris thickness patterns transition into concave-up patterns down-glacier as emergence rates and surface velocities decline toward zero (Figs. 2, 7, and 9). The numerical model—which allows for variable, declining surface velocities—reproduces this pattern (Fig. 9). Concave-up debris thickness patterns (*velocity controlled*) are therefore

the product of the typically monotonic decline of surface velocities toward the terminus.

Most debris on thick, continuously debris-covered glaciers emerges near the point of initial debris emergence where sub-debris melt rates are largest (Figs. 5 and 9). For all 144 numerical debris thickness patterns, debris emergence is largest near the up-glacier end of the debris cover (Figs. 5 and 9). Debris emergence rates are unlikely to increase toward glacier termini on any debris-covered glacier with thick debris extending to the terminus. This occurs because debris thickness almost always increases down-glacier: the melt-insulating effects of thickening debris overcomes any increase in englacial debris concentration. This re-emphasizes that once sub-debris melt is negligible englacial debris no longer emerges so the englacial debris concentration is irrelevant (Fig. 9).

5.3. Does the shape of debris thickness profiles have a primary effect on reduced surface velocity gradients of debris-covered glaciers?

Concavity of the debris thickness pattern has a negligible effect on the steady state ice thickness and surface velocity patterns of modeled glaciers (Fig. 6). Adding more and more debris to a glacier has a progressively smaller effect on the steady state mass balance, ice thickness and surface velocity pattern (Eq. (7)). These typical patterns of ice thickness and surface velocity are simply the result of continuous, thick debris (>2 cm). This occurs with largely convex-up and concave-up debris thickness profiles. Continuous, thick debris cover is all that is necessary to extend glacier termini and lower velocity, ice thickness, and ice discharge gradients.

5.4. Extending to a two-dimensional view of glacier surfaces

While we use a one-dimensional approach with a linear bed here, real glacier surfaces are two-dimensional with variable bed slopes and multiple accumulation basins. If we treat our one-dimensional debris patterns as representations of a single streamline we can gain insight into two-dimensional patterns. Lateral surface flow can be accounted for by adding an additional term to Eq. (9):

$$\frac{\partial h_{debris}}{\partial t} = \frac{Cb'}{(1-\phi)\rho_r} - \frac{\partial (U_x h_{debris})}{\partial x} - \frac{\partial (U_y h_{debris})}{\partial y} \tag{29}$$

where U_x is the longitudinal, down-glacier ice surface speed; U_y is the transverse component of surface flow; and dy is a transverse distance. We neglect lateral shear strain rates (see Van der Veen, 2013). Wherever the surface strain rate is net divergent ($\partial U_x/\partial x + \partial U_y/\partial y > 0$, debris will thin; and wherever the surface strain rate is net convergent ($\partial U_x/\partial x + \partial U_y/\partial y < 0$, debris will thicken.

Valley glacier surface streamlines tend to diverge in the ablation zone as longitudinal flow is reduced toward the margin and lateral flow increases (Raymond, 1971; Hooke, 1998; Fig. 10). Profiles in Fig. 2 support the dominance of convergent flow along central streamlines in the ablation zone. It follows that convergent flow would also dominate on off-center streamlines as well (e.g., Hooke, 1998). Debris thickness maps from Bara Shigri, Rakhiot, Khumbu, Koxkar, Panchhi Nala, Qingbingtan, and Vernerocolo glaciers show thin debris in the glacier center, with thicker debris away from the center and then thinner debris again near the glacier margin (Fig. 10; Owen et al., 2003; Juen et al., 2014; Rounce and McKinney, 2014; Bochiola et al., 2015;

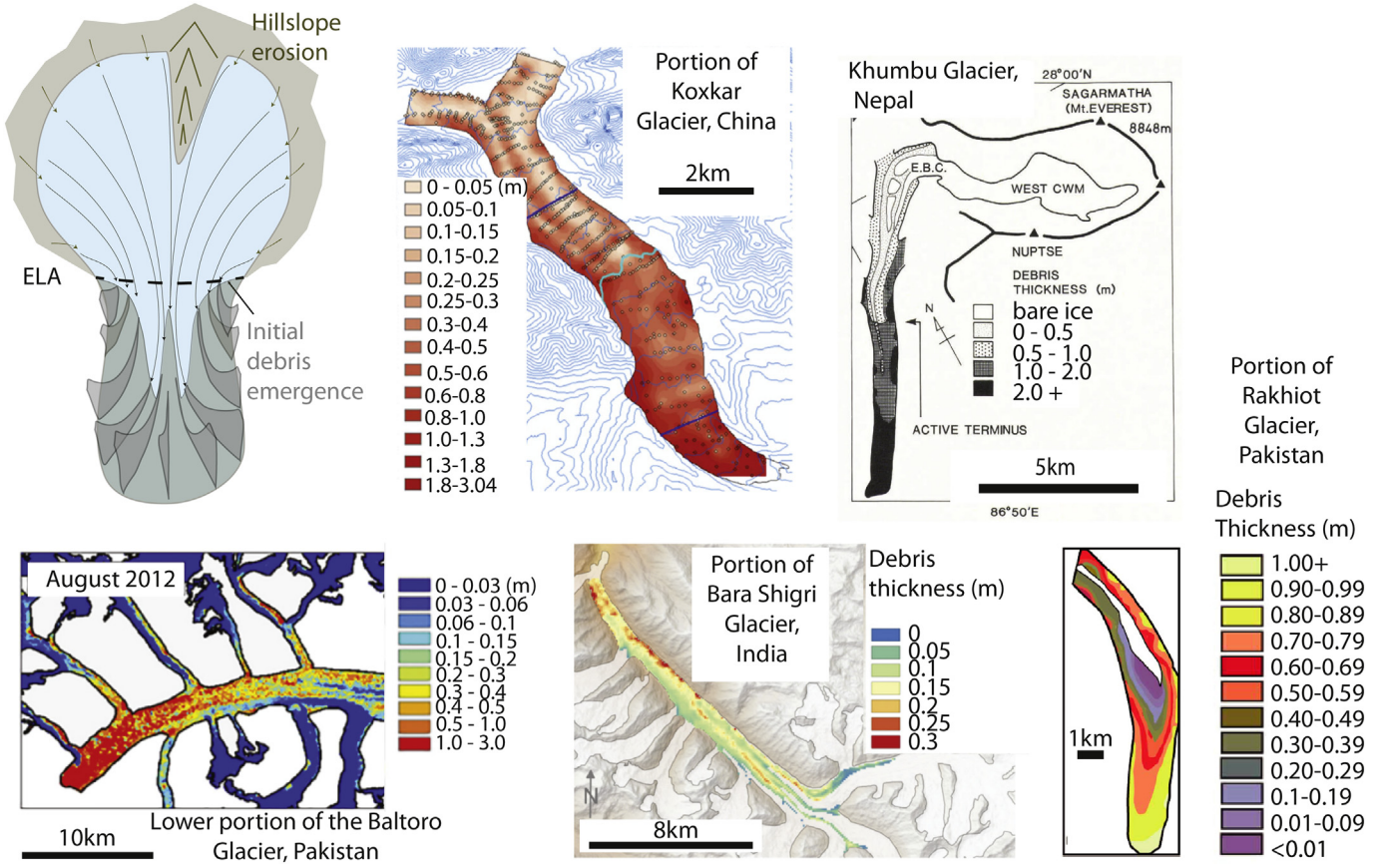

Fig. 10. Extrapolating our one-dimensional results to two-dimensions. Upper left: Schematic of concave-up one-dimensional debris profiles along flowlines. Debris thicknesses clockwise from the Koxkar glacier example: Huang et al., 2018; Nakawo et al., 1986; Owen et al., 2003; Schauwecker et al., 2015; Gibson et al., 2017. See Garg et al. (2017) for an additional example. Portions of figure reproduced with permission from John Wiley and Sons, Elsevier, and Cambridge University Press.

Schauwecker et al., 2015; Garg et al., 2017; Wang et al., 2017; Huang et al., 2018). Debris thinning on the final descent to the glacier edge could be the result of divergent flow and the typical convex-up transverse surface profile observed on valley glaciers. Steep slopes at the edge of glaciers also promote the wasting of debris off-glacier (e.g., Hooke, 1998).

Short flow paths imply near-*ELA* initial-debris emergence (Fig. 10 schematic). Given a uniform input of debris at the headwall, moving down-glacier from the *ELA* debris will tend to emerge first near the glacier margin and last near the glacier interior (Fig. 10; e.g., Nakawo et al., 1986; Owen et al., 2003; Wang et al., 2017). Flowlines will first show a convex-up debris profile that transitions to a concave-up pattern down-glacier with potentially decreasing debris thicknesses near the glacier edge (Fig. 9).

5.5. Other controls on debris thickness patterns

Debris supply, climate change, and glacier geometry also effect debris patterns, but they typically ornament the observed *velocity controlled* pattern (Figs. 2 and 10).

5.5.1. Secondary effect on debris convexity: nonuniform glacier geometry

Here, nonuniform glacier geometry refers to variability in glacier bed slope and width. Glaciers with multiple accumulation basins will tend to form ice-stream interaction medial moraines (e.g., Anderson, 2000; Gibson et al., 2017). These medial moraines result from the concentration of debris into septa. *Velocity dominance* still leads to convex-concave-up debris thickness patterns on glaciers with medial moraines (see the Ayutor-2, Baltoro, Kennicott, Koxkar, and Pasterze glaciers). Coalescing debris-covered tributaries may lead to across-glacier debris thickness variations (e.g., Baltoro glacier; Minora et al., 2015; Gibson et al., 2017), but individual flow lines will still evolve toward a convex-concave shape.

Debris thinning will occur where flow accelerates in the ablation zone, for example, at the up-glacier end of an ice fall (Fig. 8; see Hailuogou glacier and Zhang et al., 2011). Debris will also be lost in ice falls by wasting into crevasses that could reduce debris thicknesses. These effects are secondary considering the monotonic increase of debris for most observed debris profiles (Fig. 2). Local, minor debris thickening is expected at tributary junctions where flow convergence occurs (Gudmundsson, 1999; Anderson, 2000) and at the base of ice falls. Individual flowlines with debris cover will evolve toward the convex-concave profile.

5.5.2. Secondary effect on convexity: climate change

Climate change appears to primarily effect debris cover extent: debris covers are expanding globally because of rising temperatures (e.g., Kirkbride, 1993, 2000; Deline, 2005; Garg et al., 2017). On the decadal timescale, a warming climate leads to reduced surface velocity gradients and the preservation of the shape of longitudinal debris profiles (e.g., Kirkbride, 1995; Naito et al., 2000; Quincey et al., 2009; Crump et al., 2017). Increasing the air temperature above a thick debris cover is unlikely to produce large increases in sub-debris melt and sub-debris emergence rates (e.g., Brock et al., 2010). Following Kirkbride (2000) cooling should lead to faster ice flow, lower ice ablation, and the subsequent contraction of debris cover extent. Climate likely affects debris profile shape through its control of hillslope erosion (see Stoffel and Huggel, 2012; Scherler, 2014; Deline et al., 2015). We are not aware of a scenario where climate can disrupt the evolution of debris thickness patterns toward a convex- concave-up profile.

5.5.3. Secondary effect on debris convexity: variable debris supply

Rock type, bedrock fracture density, and topographic slope all strongly control hillslope erosion rate (e.g., Anderson and Anderson, 2010). Higher debris supply to one flowline will lead to thicker debris than on a flowline with lower debris supply, although both will evolve toward the convex-concave debris thickness pattern if debris supply is even quasi-steady.

Nonsteady debris supply, in which debris supply varies in time, will lead to bulges in debris thickness profiles that are superimposed on the convex-concave debris pattern (Figs. 2C and 10; see Owen et al., 2003; Deline, 2005; Mihalcea et al., 2008; Reznichenko et al., 2011; Shugar and Clague, 2011; Deline et al., 2015; Schauwecker et al., 2015). Glaciers with longer debris residence times are more likely to record variations in debris supply. Differences in the characteristics of the debris layer itself (h_*, density, and porosity) are not likely to affect the convex-concave shape (numerical simulations; Fig. 2). We expect that nonsteady debris supply is the primary control of perturbations to the expected convex-concave pattern (see Deline, 2005; Mihalcea et al., 2008; Hewitt, 2009; Deline et al., 2015).

6. Conclusions

The reduction of debris emergence rate down-glacier produces convex-up debris thickness patterns (*ablation controlled*), whereas the down-glacier reduction in surface velocity (*velocity controlled*) leads to concave-up debris thickness patterns. This convex-concave debris pattern is observed on most debri
s-covered glaciers and is the result of processes inherent to all valley glaciers. It is most likely that deviations from this pattern are caused by nonsteady debris supply to the glacier. The establishment of this background, expected debris thickness pattern allows us to identify cases in which debris delivery has varied in time and presents a baseline from which the effects of climate change on debris cover can be better quantified.

Acknowledgements

We acknowledge financial support from NSF award EAR-1548725 to R.S.A., and NSF award DGE-1144083 (GRFP) and a Murie Science and Learning Center Fellowship to L.S.A. We are grateful to Richard Marston for thoughtful, patient editing. We thank Dirk Scherler and an anonymous reviewer for comments that greatly improved the manuscript. We thank Peter Molnar and Gerard Roe for initial discussions that led to this work, and William Armstrong for carefully reading of an earlier version of this manuscript.

References

Anderson, R.S., 2000. A model of ablation-dominated medial moraines and the generation of debris-mantled glacier snouts. J. Glaciol. 46, 459–469.
Anderson, L.S., 2014. Glaicer Response to Climate Change: Modeling the Effects of Weather and Debris-Cover. University of Colorado-Boulder.
Anderson, R.S., Anderson, S.P., 2010. Geomorphology: The Mechanics and Chemistry of Landscapes. Cambridge University Press.
Anderson, L.S., Anderson, R.S., 2016. Modeling debris-covered glaciers: extension due to steady debris input. Cryosphere 10:1105–1124. https://doi.org/10.5194/tcd-9-6423-2015.
Anderson, R.S., Molnar, P., Kessler, M.A., 2006. Features of glacial valley profiles simply explained. J. Geophys. Res. Earth Surf. 111.
Azzoni, R.S., Fugazza, D., Zerboni, A., Senese, A., D'Agata, C., Maragno, D., Carzaniga, A., Cernuschi, M., Diolaiuti, G.A., 2018. Evaluating high-resolution remote sensing data for reconstructing the recent evolution of supra glacial debris. Prog. Phys. Geogr. https://doi.org/10.1177/0309133317749434 (30913331774943).
Banerjee, A., Shankar, R., 2013. On the response of Himalayan glaciers to climate change. J. Glaciol. 59, 480–490.
Benn, D.I., Bolch, T., Hands, K., Gulley, J., Luckman, A., Nicholson, L.I., Quincey, D., Thompson, S., Toumi, R., Wiseman, S., 2012. Response of debris-covered glaciers in the Mount Everest region to recent warming, and implications for outburst flood hazards. Earth Sci. Rev. 114:156–174. https://doi.org/10.1016/j.earscirev.2012.03.008.
Bochiola, D., Senese, A., Mihalcea, C., Mosconi, B., D'Agata, C., Smiraglia, C., Diolaiuti, G., 2015. An ablation model for debris-covered ice: the case study of venerocolo glacier (Italian Alps). Geogr. Fis. e Din. Quat. 38:113–128. https://doi.org/10.4461/GFDQ.2015.38.11.
Bolch, T., Buchroithner, M., Pieczonka, T., Kunert, A., 2008. Planimetric and volumetric glacier changes in the Khumbu Himal, Nepal, since 1962 using corona, Landsat TM and ASTER data. J. Glaciol. 54:592–600. https://doi.org/10.3189/002214308786570782.
Brock, B.W., Mihalcea, C., Kirkbride, M.P., Diolaiuti, G., Cutler, M.E.J., Smiraglia, C., 2010. Meteorology and surface energy fluxes in the 2005–2007 ablation seasons at the

Miage debris-covered glacier, Mont blanc massif, Italian alps. J. Geophys. Res. 115: D09106. https://doi.org/10.1029/2009JD013224.
Buri, P., Pellicciotti, F., Steiner, J.F., Miles, E.S., Immerzeel, W.W., 2016. A grid-based model of backwasting of supraglacial ice cliffs on debris-covered glaciers. Ann. Glaciol. 57: 199–211. https://doi.org/10.3189/2016AoG71A059.
Clark, D.H., Clark, M.M., Gillespie, A.R., 1994. Debris-covered glaciers in the Sierra Nevada, California, and their implications for snowline reconstructions. Quat. Res. 41, 139–153.
Crump, S.E., Anderson, L.S., Miller, G.H., Anderson, R.S., 2017. Interpreting exposure ages from ice-cored moraines: a Neoglacial case study on Baffin Island, Arctic Canada. J. Quat. Sci. 32, 1049–1062.
Deline, P., 2005. Change in surface debris cover on Mont Blanc massif glaciers after the "Little Ice Age" termination. The Holocene 15, 302–309.
Deline, P., 2009. Interactions between rock avalanches and glaciers in the Mont Blanc massif during the late Holocene. Quat. Sci. Rev. 28:1070–1083. https://doi.org/10.1016/j.quascirev.2008.09.025.
Deline, P., Hewitt, K., Reznichenko, N., Shugar, D., 2015. Rock avalanches onto glaciers. Landslide Hazards, Risks, and Disasters:pp. 263–319 https://doi.org/10.1016/B978-0-12-396452-6.00009-4.
Eyles, N., Rogerson, R.J., 1978. A framework for the investigation of medial moraine formation: Austerdalsbreen, Norway, and Berendon Glacier, British Columbia, Canada. J. Glaciol. 20, 99–113.
Garg, P.K., Shukla, A., Jasrotia, A.S., 2017a. An integrated field and remote sensing based approach for estimating influence of debris thickness on glacier surface elevation changes. International Geoscience and Remote Sensing Symposium, pp. 2840–2843.
Garg, P.K., Shukla, A., Tiwari, R.K., Jasrotia, A.S., 2017b. Assessing the status of glaciers in part of the Chandra basin, Himachal Himalaya: a multiparametric approach. Geomorphology 284:99–114. https://doi.org/10.1016/j.geomorph.2016.10.022.
Gibson, M.J., Glasser, N.F., Quincey, D.J., Mayer, C., Rowan, A.V., Irvine-Fynn, T.D.L., 2017. Temporal variations in supraglacial debris distribution on Baltoro Glacier, Karakoram between 2001 and 2012. Geomorphology 295:572–585. https://doi.org/10.1016/j.geomorph.2017.08.012.
Glazyrin, G., 1975. The formation of ablation moraines as a function of the climatological environment. Int. Assoc. Hydrol. Sci. 104, 106–110.
Gudmundsson, G.H., 1999. A three-dimensional numerical model of the confluence area of Unteraargletscher, Bernese Alps, Switzerland. J. Glaciol. 45:219–230. https://doi.org/10.3189/002214399793377086.
Hewitt, K., 2009. Rock avalanches that travel onto glaciers and related developments, Karakoram Himalaya, Inner Asia. Geomorphology 103:66–79. https://doi.org/10.1016/j.geomorph.2007.10.017.
Hooke, R.L., 1998. Principles of Glacier Mechanics. 1st ed. Prentice Hall, Upper Saddle River, New Jersey.
Huang, L., Li, Z., Han, H., Tian, B., Zhou, J., 2018. Analysis of thickness changes and the associated driving factors on a debris-covered glacier in the Tienshan Mountain. Remote Sens. Environ. 206:63–71. https://doi.org/10.1016/j.rse.2017.12.028.
Janke, J.R., Bellisario, A.C., Ferrando, F.A., 2015. Classification of debris-covered glaciers and rock glaciers in the Andes of central Chile. Geomorphology 241:98–121. https://doi.org/10.1016/j.geomorph.2015.03.034.
Juen, M., Mayer, C., Lambrecht, A., Han, H., Liu, S., 2014. Impact of varying debris cover thickness on ablation: a case study for Koxkar Glacier in the Tien Shan. Cryosphere 8:377–386. https://doi.org/10.5194/tc-8-377-2014.
Kellerer-Pirklbauer, A., 2008. The supraglacial debris system at the Pasterze glacier, Austria: spatial distribution, characteristics and transport of debris. Zeitschrift für Geomorphol. Suppl. Issues 52:3–25. https://doi.org/10.1127/0372-8854/2008/0052S1-0003.
Kirkbride, M.P., 1993. The temporal significance of transitions from melting to calving termini at glaciers in the central Southern Alps of New Zealand. The Holocene 3: 232–240. https://doi.org/10.1177/095968369300300305.
Kirkbride, M.P., 1995. Ice flow vectors on the debris-mantled Tasman glacier, 1957–1986. Geogr. Ann. Ser. A Phys. Geogr. 77, 147–157.
Kirkbride, M., 2000. Ice-marginal geomorphology and Holocene expansion of debris-covered Tasman Glacier, New Zealand. IAHS Publ. 211–217.
Kirkbride, M.P., Deline, P., 2013. The formation of supraglacial debris covers by primary dispersal from transverse englacial debris bands. Earth Surf. Process. Landforms 38: 1779–1792. https://doi.org/10.1002/esp.3416.
Kirkbride, M.P., Warren, C.R., 1999. Tasman Glacier, New Zealand: 20th-century thinning and predicted calving retreat. Glob. Planet. Change 22:11–28. https://doi.org/10.1016/S0921-8181(99)00021-1.
Konrad, S.K., Humphrey, N.F., 2000. Steady-state flow model of debris-covered glaciers (rock glaciers). Debris-Covered Glaciers: Proceedings of an International Workshop Held at the University of Washington in Seattle, Washington, USA, 13–15 September 2000. IAHS Publ, pp. 255–266.
Menounos, B., Clague, J.J., Clarke, G.K.C., Marcott, S.A., Osborn, G., Clark, P.U., Tennant, C., Novak, A.M., 2013. Did rock avalanche deposits modulate the late Holocene advance of Tiedemann glacier, southern Coast Mountains, British Columbia, Canada? Earth Planet. Sci. Lett. 384, 154–164.
Mihalcea, C., Brock, B.W., Diolaiuti, G., D'Agata, C., Citterio, M., Kirkbride, M.P., Cutler, M.E.J., Smiraglia, C., 2008a. Using ASTER satellite and ground-based surface temperature measurements to derive supraglacial debris cover and thickness patterns on Miage glacier (Mont Blanc Massif, Italy). Cold Reg. Sci. Technol. 52:341–354. https://doi.org/10.1016/j.coldregions.2007.03.004.
Mihalcea, C., Mayer, C., Diolaiuti, G., D'Agata, C., Smiraglia, C., Lambrecht, A., Vuillermoz, E., Tartari, G., 2008b. Spatial distribution of debris thickness and melting from remote-sensing and meteorological data, at debris-covered Baltoro glacier, Karakoram, Pakistan. Ann. Glaciol. 48:49–57. https://doi.org/10.3189/172756408784700680.
Mihalcea, C., Mayer, C., Diolaiuti, G., Lambrecht, A., Smiraglia, C., Tartari, G., 2006. Ice ablation and meteorological conditions on the debris-covered area of Baltoro glacier, Karakoram, Pakistan. Ann. Glaciol. 43, 292–300.
Minora, U., Senese, A., Bocchiola, D., Soncini, A., D'agata, C., Ambrosini, R., Mayer, C., Lambrecht, A., Vuillermoz, E., Smiraglia, C., Diolaiuti, G., 2015. A simple model to evaluate ice melt over the ablation area of glaciers in the central Karakoram National Park, Pakistan. Ann. Glaciol. 56:202–216. https://doi.org/10.3189/2015AoG70A206.
Naito, N., Nakawo, M., Kadota, T., Raymond, C.F., 2000. Numerical simulation of recent shrinkage of Khuinbu Glacier, Nepal Himalayas. Debris-Covered Glaciers: Proceedings of an International Workshop Held at the University of Washington in Seattle, Washington, USA, 13–15 September 2000, p. 245.
Nakawo, M., Iwata, S., Yoshida, M., 1986. Processes which distribute supraglacial debris on the Khumbu glacier, Nepal Himalaya. Ann. Glaciol. 8:129–131. https://doi.org/10.1017/S0260305500001294.
Nicholson, L., Benn, D.I., 2006. Calculating ice melt beneath a debris layer using meteorological data. J. Glaciol. 52, 463–470.
Ogilvie, I.H., 1904. The effect of supraglacial debris on the advance and retreat of some Canadian glaciers. J. Geol. 12, 722–743.
Østrem, G., 1959. Ice melting under a thin layer of moraine, and the existence of ice cores in moraine ridges. Geogr. Ann. Ser. A, Phys. Geogr. 228–230.
Owen, L.A., Derbyshire, E., Scott, C.H., 2003. Contemporary sediment production and transfer in high-altitude glaciers. Sediment. Geol. 155:13–36. https://doi.org/10.1016/S0037-0738(02)00156-2.
Patel, L.K., Sharma, P., Thamban, M., Singh, A., Ravindra, R., 2016. Debris control on glacier thinning—a case study of the Batal glacier, Chandra basin, western Himalaya. Arab. J. Geosci. 9. https://doi.org/10.1007/s12517-016-2362-5.
Popovnin, V., Rozova, A., 2002. Influence of sub-debris thawing on ablation and runoff of the Djankuat glacier in the Caucasus: selected paper from EGS general assembly, Nice, April-2000 (symposium OA36). Hydrol. Res. 33, 75–94.
Quincey, D.J., Luckman, A., Benn, D., 2009. Quantification of Everest region glacier velocities between 1992 and 2002, using satellite radar interferometry and feature tracking. J. Glaciol. 55:596–606. https://doi.org/10.3189/002214309789470987.
Raymond, C.F., 1971. Flow in a transverse section of Athabasca glacier, Alberta, Canada. J. Glaciol. 10, 55–84.
Reznichenko, N.V., Davies, T.R.H., Alexander, D.J., 2011. Effects of rock avalanches on glacier behaviour and moraine formation. Geomorphology 132:327–338. https://doi.org/10.1016/j.geomorph.2011.05.019.
Rounce, D.R., McKinney, D.C., 2014. Debris thickness of glaciers in the Everest area (Nepal Himalaya) derived from satellite imagery using a nonlinear energy balance model. Cryosphere 8:1317–1329. https://doi.org/10.5194/tc-8-1317-2014.
Rowan, A.V., Egholm, D.L., Quincey, D.J., Glasser, N.F., 2015. Modelling the feedbacks between mass balance, ice flow and debris transport to predict the response to climate change of debris-covered glaciers in the Himalaya. Earth Planet. Sci. Lett. 430: 427–438. https://doi.org/10.1016/j.epsl.2015.09.004.
Schauwecker, S., Rohrer, M., Huggel, C., Kulkarni, A., Ramanathan, A.L., Salzmann, N., Stoffel, M., Brock, B., 2015. Remotely sensed debris thickness mapping of bara Shigri glacier, Indian Himalaya. J. Glaciol. 61:675–688. https://doi.org/10.3189/2015JoG14J102.
Scherler, D., 2014. Climatic limits to headwall retreat in the Khumbu Himalaya, eastern Nepal. Geology https://doi.org/10.1130/G35975.1.
Scherler, D., Bookhagen, B., Strecker, M.R., 2011. Hillslope-glacier coupling: the interplay of topography and glacial dynamics in high Asia. J. Geophys. Res. 116:F02019. https://doi.org/10.1029/2010JF001751.
Shroder, J.F., Shroder, J.F., Bishop, M.P., Bishop, M.P., Copland, L., Copland, L., Sloan, V.F., Sloan, V.F., 2000. Debris-covered glaciers and rock glaciers in the nanga parbat himalaya. Pakistan Geogr.:17–31 https://doi.org/10.1111/j.0435-3676.2000.00108.x.
Shugar, D.H., Clague, J.J., 2011. The sedimentology and geomorphology of rock avalanche deposits on glaciers. Sedimentology 58:1762–1783. https://doi.org/10.1111/j.1365-3091.2011.01238.x.
Shukla, A., Gupta, R.P., Arora, M.K., 2009. Estimation of debris cover and its temporal variation using optical satellite sensor data: a case study in Chenab basin, Himalaya. J. Glaciol. 55:444–452. https://doi.org/10.3189/002214309788816632.
Stoffel, M., Huggel, C., 2012. Effects of climate change on mass movements in mountain environments. Prog. Phys. Geogr. 36:421–439. https://doi.org/10.1177/0309133312441010.
Stokes, C.R., Popovnin, V., Aleynikov, A., Gurney, S.D., Shahgedanova, M., 2007. Recent glacier retreat in the Caucasus Mountains, Russia, and associated increase in supraglacial debris cover and supra-/proglacial lake development. Ann. Glaciol. 46: 195–203. https://doi.org/10.3189/172756407782871468.
Vacco, D.A., Alley, R.B., Pollard, D., 2010. Glacial advance and stagnation caused by rock avalanches. Earth Planet. Sci. Lett. 294:123–130. https://doi.org/10.1016/j.epsl.2010.03.019.
Van der Veen, C.J., 2013. Fundamentals of Glacier Dynamics. CRC Press.
Wagnon, P., Vincent, C., Arnaud, Y., Berthier, E., Vuillermoz, E., Gruber, S., Ménégoz, M., Gilbert, A., Dumont, M., Shea, J.M., Stumm, D., Pokhrel, B.K., 2013. Seasonal and annual mass balances of Mera and Pokalde glaciers (Nepal Himalaya) since 2007. Cryosphere 7:1769–1786. https://doi.org/10.5194/tc-7-1769-2013.
Wang, P., Li, Z., Li, H., Wang, W., Zhou, P., Wang, L., 2017. Characteristics of a partially debris-covered glacier and its response to atmospheric warming in Mt. Tomor, Tien Shan, China. Glob. Planet. Change 159:11–24. https://doi.org/10.1016/j.gloplacha.2017.10.006.
Wang, L., Li, Z., Wang, F., 2011. Spatial distribution of the debris layer on glaciers of the Tuomuer Peak, western Tian Shan. J. Earth Sci. 22:528–538. https://doi.org/10.1007/s12583-011-0205-6.
Yde, J.C., Paasche, O., 2010. Reconstructing climate change: not all glaciers suitable. Eos (Washington. DC) 91:189–191. https://doi.org/10.1029/2010EO210001.

Zech, R., Abramowski, U., Glaser, B., Sosin, P., Kubik, P.W., Zech, W., 2005. Late quaternary glacial and climate history of the Pamir Mountains derived from cosmogenic 10Be exposure ages. Quat. Res. 64:212–220. https://doi.org/10.1016/j.yqres.2005.06.002.

Zhang, Y., Fujita, K., Liu, S., Liu, Q., Nuimura, T., 2011. Distribution of debris thickness and its effect on ice melt at Hailuogou glacier, southeastern Tibetan Plateau, using in situ surveys and ASTER imagery. J. Glaciol. 57:1147–1157. https://doi.org/10.3189/002214311798843331.

Zhang, Y., Hirabayashi, Y., Fujita, K., Liu, S.Y., Liu, Q., 2016. Heterogeneity in supraglacial debris thickness and its role in glacier mass changes of the Mount Gongga. Sci. China Earth Sci. 59:170–184. https://doi.org/10.1007/s11430-015-5118-2.